# Two-Dimensional Melts: Polymer Chains at the Air−Water Interface

**Grant T. Gavranovic,[†] Joshua M. Deutsch,[‡] and Gerald G. Fuller*,[†]**

*Department of Chemical Engineering, Stanford University, Stanford, California 94305-5025, and Department of Physics, University of California, Santa Cruz, Santa Cruz, California 95064*

*Received January 11, 2005; Revised Manuscript Received May 3, 2005*

ABSTRACT: Both physical surface rheology and computer simulation experiments were performed to understand the conformation of polymers in 2D systems. The interfacial stress rheometer was used to measure surface rheological properties of Langmuir monolayers of poly(*tert*-butyl methacrylate) with molecular weights between 81.5 and 780 kg mol$^{-1}$. The $\Pi-A$ isotherms for these monolayers show two transitions: a plateau at $\Pi \approx 18$ mN m$^{-1}$ and a bend at $\Pi \approx 52$ mN m$^{-1}$. The properties of the films are shown to be substantially different above and below the plateau surface pressure, $\Pi_p$. Below $\Pi_p$, the monolayers are primarily viscous, and surface viscosity increases linearly with MW, while above $\Pi_p$, the films are more elastic, and surface viscosity is MW-independent. Computer simulations of these systems produce qualitatively similar $\Pi-A$ isotherms. The observed transition at $\Pi_p$ marks the changeover from polymer chains existing in a single layer to forming regions of multilayers.

## Introduction

When mobile polymers are confined to essentially two-dimensional (2D) conformations, the resulting systems can be thought of as analogues of conventional polymer solutions and melts. Several computer simulations have lent some insight into the molecular conformation of such constrained polymer systems;[1,2] however, relatively few experimental efforts have focused on addressing this issue. In this work, we use rheological properties of polymer monolayers and conduct additional computer simulations to better understand chain conformation in interfacial polymer systems.

It is well-known that surfactants, such as polymers, can be used to stabilize fluid−fluid systems, such as emulsions and foams.[3] In fact, polymer molecules can facilitate the formation of these structures through a number of stabilization mechanisms, including steric repulsion, electrostatic double-layer repulsion, Marangoni flow generation, and rigid-shell formation. Additionally, the same molecules can sometimes stabilize both emulsions and foams, such as asphaltene macromolecules in water−crude oil systems.[4,5] This fact illustrates that the effects of surfactants at the air/water (A/W) interface can be quite similar to those resulting from their presence at liquid/liquid interfaces. Therefore, the work discussed in this paper involving polymer monolayers at A/W has clear implications to a wide range of fluid/fluid systems.

One of the primary issues in the study of two-dimensional polymer systems is whether chain interpenetration occurs. Although chain overlap and entanglement are not possible in two dimensions, the domain occupied by an individual chain may interpenetrate the domains of neighboring chains. While de Gennes suggests[6] that chains primarily form condensed, segregated disks even at high surface concentrations, most simulations[1,2,7] have supported the idea that polymers tend to be more extended, forming an interpenetrated network.

Under the segregated disk argument, individual polymer chains exist as isolated coils that contract in size as they contact adjacent chains when concentration is increased. For 2D melts, a chain with degree of polymerization, $N$, will have a characteristic radius, $R_g$, such that the concentration of a chain, $c = NR_g^{-2}$, is comparable to the overall concentration. Thus, the radius of gyration scales with $N$ according to the relation $R_g \sim N^{\nu}$, where $\nu = 0.5$. If interpenetration of chains is considered, scaling arguments have suggested that the same dependences are coincidently obeyed.[1]

Theoretical work by Semenov and Johner considered two models for flexible chains in ultrathin geometries.[8] One system forbids crossing, while the other describes a film with some thickness and allows entanglement. These approaches result in dramatically different conclusions; however, the first model suggests that strict segregation of individual chains into disks takes place. The standard radius of gyration power-law scaling with chain length can also have a logarithmic correction, depending on the choice of model.

Another possible configuration at high surface concentrations is the collapse of the monolayer into a multilayer system. Peng and Barnes suggested that this occurs at the inflection point of the $\Pi-A$ isotherm.[9] This idea is also supported by work by Naito in which Langmuir−Blodgett films of poly(isobutyl methacrylate) (PiBMA) showed clear X-ray diffraction peaks if deposited before the inflection point.[10] However, no peaks were observed for films formed after the inflection. Naito also suggests that the carbonyl group present in this polymer will attach to the interface at low surface pressure but will detach as $\Pi$ increases. This behavior could lead to a "flipping up" of monomer units as PiBMA monolayers are compressed.

While a few 2D polymer systems have been studied under conditions other than at the air/water interface, Langmuir monolayers have been the primary subjects of investigation in this field. Perhaps the most well-known experiments in the former category are those performed by Maier and Rädler on fluorescently labeled DNA adsorbed on supported lipid bilayers.[11−13] Here, they found that $R_g \sim N^{0.74}$, nearly exactly the predicted two-dimensional Flory exponent of $\nu_F = 0.75$ for a self-

[†] Stanford University.
[‡] University of California, Santa Cruz.
* Corresponding author: e-mail ggf@stanford.edu.

10.1021/ma050061n CCC: $30.25 
Published on Web 06/25/2005

avoiding walk in 2D. However, there have also been many studies on polymers at the air/water interface. Studies of poly(methyl methacrylate) (PMMA) and poly(vinyl acetate) (PVA) monolayers by Vilanove and Rondelez[14] used scaling arguments to find $\nu = 0.56$ and 0.79, respectively, for these two systems. On the basis of these results, the authors suggest that the air/water interface behaves as a $\Theta$ solvent for PMMA and as a good solvent for PVA. With Poupinet, this group has also studied the molecular weight (MW) dependence of the second virial coefficient in 2D[15] and conducted a more in-depth study of the $\nu$ exponent in 2D.[16] Experiments conducted by Sacchetti et al.[17,18] analyzed poly(*tert*-butyl methacrylate) (PtBMA) with molecular weights of 10 and 249 kg mol$^{-1}$. The work performed by Sacchetti et al. is particularly relevant to the work presented here because it deals with the same polymer and reports surface pressure−area isotherms as well as surface viscosity data for this system at surface pressures up to $\Pi = 18$ mN m$^{-1}$. They report that surface viscosity, $\eta_s$, scales nearly linearly with polymer molecular weight for surface pressures, $\Pi = 0.5-12$ mN m$^{-1}$. Sato et al.[19] studied monolayers of poly(vinyl octanal acetal) and found a similar scaling for surface viscosity with molecular weight, namely $\eta_s \sim N^{1.3}$. These researchers also note that since no change in this scaling is observed even at molecular weights on the order of $10^6$ g mol$^{-1}$, a 2D analogue to the 3D critical entanglement molecular weight could not be found. The studies by both Sacchetti et al. and Sato et al. used canal surface viscometers. Barentin et al.[20] used a sliding-disk viscometer to investigate monolayers of poly(ethylene oxide) (PEO), and their experiments show surface viscosity increasing nonlinearly as a function of surface pressure. Recent work conducted by Monroy and co-workers[21] examined monolayers of PVA from the dilute to the concentrated regime. The focus of this work was on relaxation dynamics, but they also report that $\nu = 0.78$ in the semidilute regime. This result nearly matches that of Vilanove and Rondelez, and it again suggests that the air/water interface is a good solvent for PVA.

Viscoelasticity studies using surface light scattering by Esker et al. found that polymer monolayers under good-solvent conditions were nearly perfectly elastic.[22] Under poor-solvent conditions, the monolayers behaved as inelastic films. Using a similar technique, Cicuta and Hopkinson found several new scaling dependences involving the dilatational modulus and surface viscosity for semidilute monolayers of both synthetic polymers and proteins.[23]

In this work, we use the interfacial stress rheometer (ISR) to measure the properties of monolayers of PtBMA in conjunction with computer simulations of these systems. Specifically, we explore the dependences of surface shear viscosity and surface moduli on surface pressure and polymer molecular weight. Together with surface pressure−area isotherms, this information helps clarify the conformation of polymers confined to monolayer geometries. Computer simulations provide qualitative pictures of how equilibrium properties such as surface pressure and average chain configuration depend on parameters like polymer−polymer and polymer−interface attraction potentials. An enhanced comprehension of interfacial polymer films will aid in the understanding of the molecular interactions that give rise to viscoelasticity in two dimensions and the mechanisms by which polymers stabilize fluid−fluid interfaces.

## Experimental Methods

**Surface Rheology Experiments.** These experiments were conducted on monolayers of poly(*tert*-butyl methacrylate). Five different molecular weights were used as received from commercial sources: $M_n$ = 81.5, 131, 211.5 (all from Polymer Source), 500, and 780 kg mol$^{-1}$ (both from Fluka). Each sample has a polydispersity $M_w/M_n < 1.3$. This polymer is not appreciably soluble in water and has amphiphilic character that allows it to exist in a 2D conformation at the air/water interface. Additionally, the polymer is essentially insoluble in decane, so we would expect it to behave similarly at the oil/water interface.

Experiments were performed at room temperature ($T = 22.5 \pm 0.5$ °C) in a Teflon trough (30 cm long, 7.5 cm wide) with movable Delrin barriers (KSV). Polymers were dissolved in chloroform solution (ca. 0.3 mg mL$^{-1}$) and spread onto a purified water (Millipore Milli-Q, resistivity 18.2 MΩ·cm) subphase using a glass microsyringe. After depositing each monolayer, solvent was allowed to evaporate for at least 30 min. All monolayers were compressed and expanded at a rate of 150 mm$^2$ min$^{-1}$ in order to allow the system to remain close to equilibrium.

Surface pressures were determined using a platinum Wilhelmy plate[24] connected to a force transducer (KSV) with resolution of 4 $\mu$N m$^{-1}$. All surface rheology measurements were made using the interfacial stress rheometer described elsewhere.[25] Briefly, this method uses Helmholtz coils to generate a magnetic field gradient that is used to move a magnetic rod situated at the air/water interface. The magnetic rod is positioned between two glass walls, such that the motion of the rod creates a shear flow profile in the plane of the interface. Experiments were performed at constant surface pressure, and care was taken to ensure that the system was in the linear viscoelastic regime. Specifically, shear strains of ~2% were generated. Multiple measurements were made on the same monolayer at different surface pressures following successive compressions and equilibrations.

Additionally, a Brewster angle microscope (BAM) was used to image the monolayers at various surface pressures in the Langmuir trough. The instrument is homemade and uses a 10 mW HeNe laser (Uniphase, $\lambda = 633$ nm) as the light source. Images were collected in gray scale using a CCD camera (Hamamatsu C2400).

**Computer Simulation Experiments.** Both lattice and off-lattice Monte Carlo simulations were performed. The lattice model is less realistic but requires far less computer time and is more useful for qualitative comparison with experimental data.

The lattice model was performed on a cubic lattice with monomers situated on lattice sites separated from each other by a step length $a$. For these simulations, $a = 1$. There were $N$ chains of length $L$ that moved according to two different move sets: reptation dynamics[26] and "kink-jump" dynamics.[27] Reptation dynamics provides an efficient means for chain equilibration which has been supplemented by these local moves to further increase the mobility of the chains.

The chains have an attraction to each other and also have an attraction to a planar interfacial region as described in the following. There is a hard wall that the chains are prohibited from entering. The layer next to it has an attractive interfacial potential of depth $-v_1$ and the next layer has a depth $-v_2$. In the simulation $v_1$ is chosen to be large enough to ensure that all the monomers are tightly bound to the interfacial region. Not only are the chains self-avoiding, but they interact with each other through a nearest-neighbor attractive potential of $-w$. All energies are measured in units of $k_BT$, where $T$ is the absolute temperature.

Initially, the simulation was run with box size $b_x \times b_y \times b_z$ and hard wall boundary conditions for a reason now described. For a continuous system, the average density of chains right

next to a wall, $\rho_w$, is rigorously related to the pressure $P$ according to the relation[28] $P = \rho_w k_B T$. However, because the lattice is discrete, it is only possible to measure the density a finite distance away, so an approximate value of the pressure can be obtained by measuring $\langle \rho_1 \rangle$, the average density of the chains at points one lattice spacing from the wall. This is not exact but gives a guide to the true pressure. An exact method using a variant of the wall density method has been given[29] and can be used to obtain pressure isotherms.

We choose instead to do simulations in a constant-pressure ensemble to obtain quantitative measurements of the pressure which also include the effects of hysteresis. In this approach, the system is simulated at constant pressure by changing the volume $V$ of the container while keeping the pressure $P$ constant. The Hamiltonian is now modified by adding a term $PV/k_BT$. The volume $V$ is equal to the number of accessible lattice sites. Again, the lattice spacing has been set to unity. At constant pressure, there is a small equilibrium fluctuation in $V$, so the volume does not change monotonically due to thermal fluctuations. For large systems, the equivalence of the constant pressure and constant volume ensembles is well established.[30]

Because the lattice is discrete, it is not possible to change $V$ by an arbitrarily small amount. If an entire plane is moved, the probability of acceptance of such a move would become exponentially small in the system size. To solve this problem, the simulation attempts to make moves that increment or decrement $V$ by a single lattice site. The lattice sites are linearly ordered using "skew boundary conditions". A lattice site with coordinates $x, y, z$ is mapped directly onto the volume by the formula $V = z + b_x(x + b_y y)$. This means as $V$ is varied, $z$ changes most rapidly, then $x$, and then $y$. Therefore, the system can be compressed by building up impenetrable columns perpendicular to the interface that exclude system chains. If an entire column is built up, the next step is to start building another one next to it. This proceeds until an entire plane is filled, when the filling of a new plane begins. The moves that allow $V$ to change also satisfy the Metropolis criterion to ensure detailed balance.

In a variant of this method which has faster equilibration times, the pressure used in the Metropolis algorithm is a function of $z$, and this pressure averaged over $z$ is equal to the homogeneous pressure $P$ used above. This is useful because almost all of the monomers are close to the interface and therefore have small values of $z$. As a result of this approach, the polymers exert an inhomogeneous force on the walls. With a constant vertical pressure, a potential barrier must be crossed when adding a column. By adjusting the pressure to be zero a few layers away from the interface, this barrier height can be diminished, and the position of the columns can vary more rapidly.

The pressure $P$ is then slowly varied so that the system is close to equilibrium. These systems will not be truly in equilibrium because, both theoretically and experimentally, they show hysteresis. However, if the system is equilibrated at a certain pressure for long enough, hysteresis will eventually go away, although this may correspond to an unrealistic experimental time scale. In the simulations, the pressure is maintained at a given value for long enough so that the average volume appears to have reached a constant value. The volume is measured as a function of time, and these measurements are divided into eight time windows. In each window, the average volume is determined. The simulation then calculates the standard deviation of these eight values and divides by the average volume. Simulations were typically run for enough steps such that this error was less than 0.03. Simulations were also performed by changing the pressure at different rates and comparing results as an additional test. This often proved to be more useful because it allowed us to control the size of the hysteresis loops in the simulated isotherms.

We also implemented Dickman's method[29] and verified that the results of the two approaches are in good agreement.

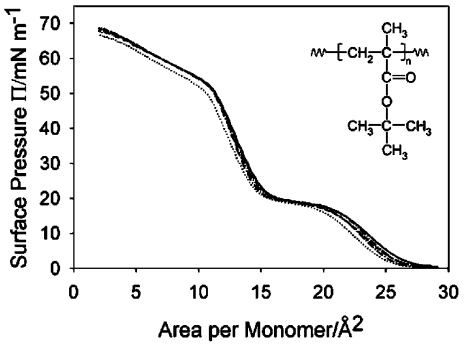


**Figure 1.** Π−*A* isotherms of PtBMA with $M_n$ = 81.5K (—), 131K (· · ·), 211K (- - -), 500K (- ·· -), and 780K (- · -) collapsing to a single curve with a plateau at Π ≈ 18 mN m$^{-1}$. Inset: monomer unit of PtBMA.

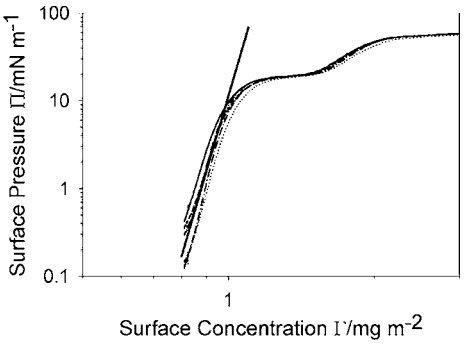


**Figure 2.** Π−Γ isotherms of PtBMA with $M_n$ = 81.5K (—), 131K (· · ·), 211K (- - -), 500K (- ·· -), and 780K (- · -) showing scaling fit in semidilute regime. The included power law fit indicates $\nu \approx 0.53$.

## Results and Discussion

**Surface Pressure−Area Isotherms.** We show the Π−*A* isotherms for PtBMA of five different molecular weights in Figure 1. The curves are in good agreement with those reported elsewhere[18] and provide a reasonable estimate for the actual size of a monomer unit. When plotted against area per monomer, all the isotherms essentially collapse onto a single curve over the full range of areas studied. The apparent horizontal displacement between some curves most likely results from small errors in dilution during solution preparation. The fact that the curves coincide suggests that each monolayer behaves similarly during compression when considered on the monomer level, regardless of the full length of each chain. In contrast to previous work, we compress our monolayers to higher pressures and observe a plateau when Π ≈ 18 mN m$^{-1}$ as well as a sudden change in slope when Π ≈ 52 mN m$^{-1}$. We call the value at which the former feature occurs the plateau surface pressure, $\Pi_p$, and interpret this behavior to indicate a monolayer phase transition. Rheology measurements discussed later reflect significant changes in monolayer properties as this plateau is crossed. It is also interesting that the high-Π regions of the isotherms, when extrapolated, intersect the surface pressure axis at 72.8 ± 0.7 mN m$^{-1}$. This value is the maximum possible surface pressure for an air/water system since it corresponds to zero surface tension.

An alternate method for presenting these isotherms, where surface pressure is plotted against surface concentration, Γ, is shown in Figure 2. When plotted in this fashion, the slope of the isotherm has been shown[14] to be related to the scaling exponent, $\nu$. For instance, in

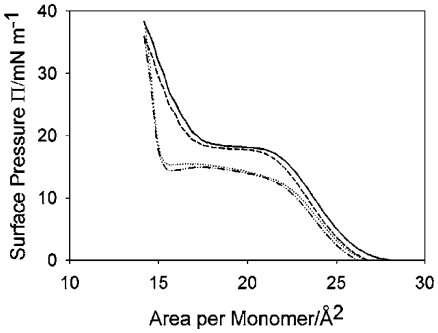


**Figure 3.** Π−*A* isotherms for PtBMA ($M_n$ = 780K) during two cycles of compression and expansion showing hysteresis. The first (—) and second (- - -) compressions are similar, as are the first (· · ·) and second (- ·· -) expansions.

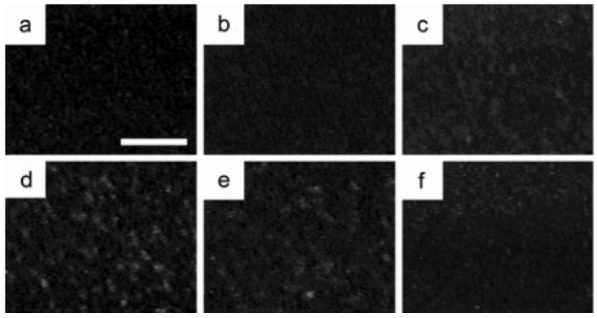


**Figure 4.** Brewster angle microscopy images of a PtBMA ($M_n$ = 780K) during compression, when Π = 13 (a), 25 (b), and 33 mN m$^{-1}$ (c), and expansion, when Π = 25 (d), 17 (e), and 13 mN m$^{-1}$ (f). The rough texture formed by compression to high Π persists to lower Π values during expansion. Scale bar = 125 $\mu$m.

the semidilute regime, $\Pi \sim \Gamma^2\nu/(2\nu - 1)$, while Π is independent of Γ in the concentrated regime. For 0.8 < Π < 5 mN m$^{-1}$, corresponding to the semidilute regime, the slopes of the isotherms suggest $\nu \approx 0.53$. This value for $\nu$ implies that the A/W interface behaves as a near-Θ solvent for PtBMA at low Γ.

Hysteresis studies were also conducted on several PtBMA monolayers, and a representative series of isotherms are presented in Figure 3. Two cycles of compression and expansion were applied, and the system was allowed to equilibrate for ∼5 min between cycles. Upon expanding the barriers following the first compression, the resulting isotherm showed a similar shape, with a decreased plateau pressure. Despite having a similar shape, a fairly large hysteresis loop is seen between the compression and expansion curves. The second compression/expansion cycle closely retraces the curves generated during the first cycle, although slightly shifted to lower areas. We attribute this difference to a small amount of leakage under the barriers. Also, during expansions, a small dip is observed as the system enters the plateau region. This feature and the lower expansion plateau pressure likely result from the monolayer not being able to redisperse as quickly as the barriers are expanding. This sort of dynamic effect does not seem to be a problem during compression.

Several PtBMA monolayer systems were also observed using Brewster angle microscopy, and representative images are shown in Figure 4. Throughout a full cycle of compression and expansion, no clear domains were observed. At low surface pressures, the films appeared homogeneous. However, when the film was compressed to Π > 25 mN m$^{-1}$, the surface began to appear somewhat rough. The maximum surface pressure reached was ∼35 mN m$^{-1}$. During expansion, the textured appearance of the film persisted through the small dip discussed previously, until the expansion plateau region was reached. Almost no structure was visible when the surface pressure was Π = 16.7 mN m$^{-1}$. The same behavior was observed on three consecutive compression−expansion cycles.

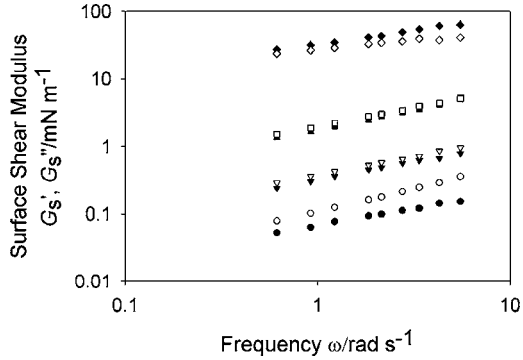


**Figure 5.** Surface shear storage (solid symbols) and loss (open symbols) moduli as functions of frequency for PtBMA ($M_n$ = 211K) when Π = 10 (●), 15 (▼), 17 (■), and 20 mN m$^{-1}$ (◆). As Π increases, the monolayer becomes more elastic, and $G_s'$ exceeds $G_s''$ when Π > $\Pi_p$.

**Rheology Measurements.** To determine the rheological properties of the PtBMA monolayers, we use the ISR to perform two types of experiments: oscillatory shear and creep compliance. From the former experiments, we measure the surface shear storage and loss moduli, $G_s'$ and $G_s''$, as functions of frequency, $\omega$. From the latter, we evaluate the surface shear viscosity, $\eta_s$.

Oscillatory shear experiments were performed at surface pressures from 1 to 20 mN m$^{-1}$, and a representative figure presenting our results is shown in Figure 5. For values of Π below $\Pi_p$, $G_s''$ is always greater than $G_s'$, indicating that, while the monolayer has both viscous and elastic character, the viscous component is more significant. Near $\Pi_p$, the values of the two surface moduli are essentially equal. No characteristic crossover frequency could be determined between PtBMA samples with different molecular weights. Finally, when Π exceeds $\Pi_p$, the surface storage modulus exceeds the surface loss modulus, marking a transition to a regime where the elastic character of the film dominates. This change further supports the idea that the PtBMA monolayers are undergoing a transition around the plateau surface pressure.

Creep compliance experiments involve applying a constant stress to the magnetic rod and monitoring the strain response of the rod as it reacts to this force. The data collected can then be fit to a viscoelastic model in order to determine the physical properties of the system. A diagram presenting a typical creep compliance response is shown in Figure 6. This figure shows creep compliance, $J$ = strain/stress, plotted vs time for a monolayer of PtBMA at constant surface pressure. The model is shown to provide an accurate fit to these data.

A representative plot of surface shear viscosity vs surface pressure is included in Figure 7. From this diagram, it is clear that the scaling dependence of $\eta_s$ on Π changes sharply at $\Pi_p$. Below $\Pi_p$, $\eta_s \sim \Pi^{2.3}$, while the dependence is much stronger above the plateau pressure. Again, this suggests the behavior of the monolayers changes dramatically when the plateau surface pressure is crossed.

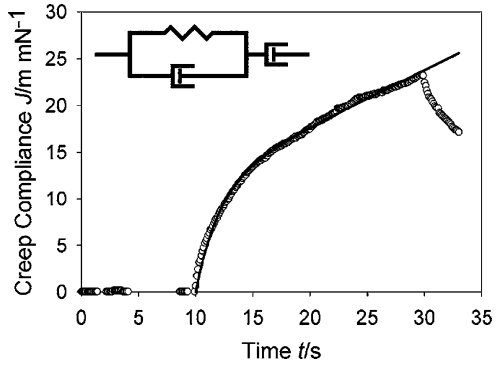


**Figure 6.** Representative creep compliance curve showing both the real response of a PtBMA monolayer ($M_n$ = 500K) (○) and the viscoelasticity model fit (—). Stress is applied from time equals 10−30 s. Inset: spring and dashpot system used to model creep compliance data.

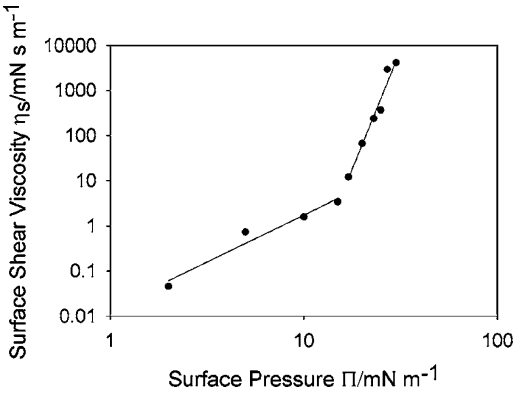


**Figure 7.** Surface shear viscosity of PtBMA ($M_n$ = 780K) as a function of surface pressure showing a change in scaling at $\Pi_p$.

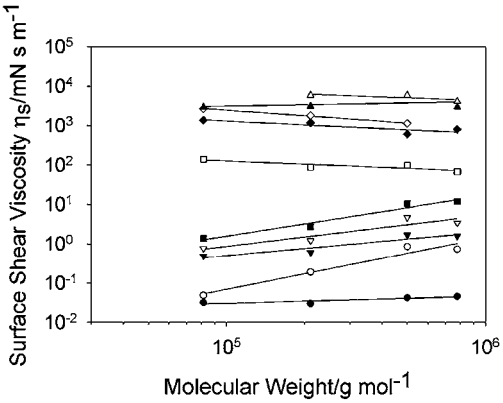


**Figure 8.** Surface shear viscosity of PtBMA as a function of molecular weight at various surface pressures. From bottom to top, Π = 2, 5, 10, 15, 17, 20, 23, 25, 27, and 30 mN m$^{-1}$. When 5 < Π < 17 mN m$^{-1}$, $\eta_s \sim$ MW[1]. Elsewhere, surface shear viscosity is essentially independent of molecular weight.

Results for $\eta_s$ over a range of surface pressures and polymer molecular weights are shown in Figure 8. The surface shear viscosity is seen to increase consistently with increasing surface pressure. Interestingly, three scaling regimes are observed to govern different surface pressure ranges. At the lowest value of surface pressure, Π = 2 mN m$^{-1}$, $\eta_s$ is essentially independent of molecular weight. For surface pressures greater than this value but below $\Pi_p$, $\eta_s$ increases linearly with MW. As mentioned previously, this relationship has been observed by other researchers for both PtBMA[17] and other polymer[19] monolayers. However, once Π exceeds $\Pi_p$, we observe that $\eta_s$ is again essentially independent of MW. This change in scaling is an additional indication of the transition that takes place at $\Pi_p$.

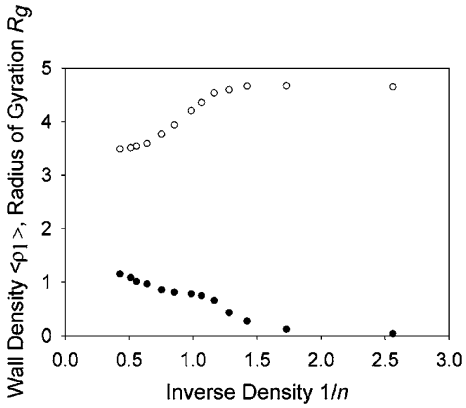


**Figure 9.** Wall density (●) and radius of gyration (○) as functions of inverse density. Both curves show transitions near complete monolayer coverage, 1/$n$ = 1.

**Computer Simulation Experiments.** The use of computer simulations allowed us to observe such properties as chain conformation and surface pressure−area values for a wide variety of system parameters.

Using the constant-volume approach, we measured various equilibrium quantities as a function of chain concentration. The results presented here are for a system with a cubic box size $b$ = 32, chain length $L$ = 16, a single attractive layer (i.e. $v_2$ = 0), $v_1$ = 2, and $w$ = 1. The values for $v_1$ and $w_1$ were large enough to ensure that the chains were strongly bound to the interfacial region.

The systems were equilibrated for 4 × 10$^8$ steps before measurements were taken. At this point, 40 000 measurements were taken with a gap of 65 536 steps between measurements. The error bars for $\langle\rho_1\rangle$ were estimated to be typically less than a percent.

In Figure 9 we plot the average radius of gyration, $\langle R_g\rangle$, as a function of inverse density, 1/$n$. This two-dimensional density $n$ is the number of chains per unit area, $n = N/b^2$. Therefore, the horizontal axis represents the average number of monomers per unit area. This figure also presents the average density of chains in the layer adjacent to a box side, $\langle\rho_1\rangle$, which is approximately related to the pressure as described previously. There is a small decrease in $\langle R_g\rangle$ as a function of chain concentration, indicating that the chains become more compact as the density increases. The variation of $\langle\rho_1\rangle$ is much stronger. There is a weak plateau region seen around $n$ = 1, which is where the chains completely fill the attractive layer.

Figure 10 shows the average density as a function of distance away from a wall, $x$, averaged over the $y$- and $z$-directions. Note that the density is lower near the walls as expected, but it shows interesting changes as a function of the number of chains. For this system, 64 chains would represent complete filling of the attractive well. Around this value, the density becomes quite flat in the middle. For lower densities and higher densities, it is more curved.

The most meaningful results we obtained were those in which the simulation was conducted at constant pressure with a "pusher" barrier to model the method of compression used in the physical experiments.

Figure 11 shows the Π−$A$ isotherms for a system with a single attractive layer. The parameters are such that

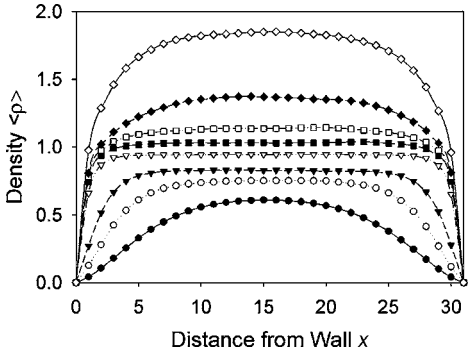


**Figure 10.** Average density in the $x$-direction as a function of distance from walls. Different curves represent different numbers of simulated chains. From top to bottom, $N = 100$, 75, 65, 60, 55, 45, 37, and 25.

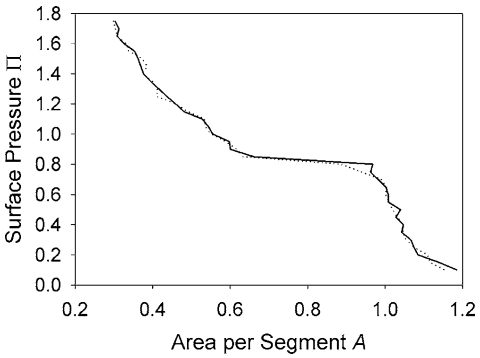


**Figure 11.** Simulated $\Pi-A$ isotherm cycle for a system with a single attractive layer showing no hysteresis. Both compression (—) and expansion (· · ·) curves are shown. In this simulation, $\Pi$ was the independent variable.

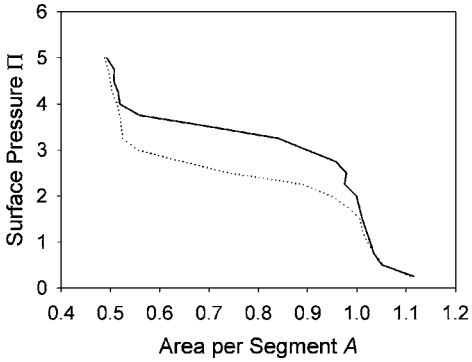


**Figure 12.** Simulated $\Pi-A$ isotherm cycle for a system with two attractive layers. Compression (—) and expansion (· · ·) curves are shown, showing a hysteresis loop that is qualitatively similar to those observed physically. In this simulation, $\Pi$ was the independent variable.

a clear plateau is seen. The parameters are $L = 16$, $b_x = 32$, $b_y = 16$, $b_z = 8$, $N = 20$, $T = 1$, $v_1 = -2.5$, and $w = -1.25$. The system was run with $2 \times 10^7$ total moves between tests for convergence as described above. The criterion for acceptance was an error less than 0.025. With this many time steps, there is hardly any hysteresis seen.

In contrast, Figure 12 shows a hysteresis loop for a system with two attractive layers. The parameters are such that a plateau is seen and the behavior at higher pressures shows similar features to the physical experiments. The parameters for this trial are $L = 16$, $b_x = 64$, $b_y = 16$, $b_z = 8$, $N = 20$, $T = 1$, $v_1 = -6$, $v_2 = -1.5$, and $w = -1$. In this case, a hysteresis loop can be seen because the energies involved were larger, corresponding to much smaller Boltzmann factors for leaving a layer. Overall, this suggests that the dynamics are far slower and would require many more orders of magnitude computer time to remove the hysteretic effects. The shapes of these isotherms are qualitatively similar to those observed experimentally.

Figure 13 shows a series of images from the simulation illustrating how the pusher functions and the polymer conformations that result. At large area, the chains generally form a single layer with several vacancies and multilayer regions existing due to finite temperature effects. When the system is compressed to high surface pressure, a multilayer network results.

Using the density at the wall of the system, a surface pressure can be calculated for a wide range of available areas. Currently, the values predicted by the computer simulation are not quantitatively accurate, but the shapes of the $\Pi-A$ isotherms obtained are qualitatively similar to those observed physically. An illustration of this is shown in Figure 14. To compare the shapes of the isotherms, the simulation isotherm has been scaled horizontally and vertically to provide the best fit to the experimental curve, and it demonstrates several key features that correspond to the physically measured isotherm. For instance, there is a clear plateau formed, and the width of the plateau is in approximately in proportion to the slopes of the isotherm above and below the plateau pressure. Also, the computer simulation curve seems to predict the change in slope seen when $\Pi \approx 52$ mN m$^{-1}$ in the experimental isotherm, however at a slightly lower pressure. The arrow in Figure 14 marks the point in the simulation where the system contains an equal number of chain segments and single-plane lattice sites. Interestingly, this point is near the inflection point of the isotherm, which has been suggested to be the point when monolayer collapse occurs, as mentioned previously. Also, this point corresponds to a mean monomer area of ~23 Å$^2$, which is a reasonable estimate for the projected area of a monomer unit of PtBMA. Naito[10] has previously estimated the size of a PiBMA monomer to be 20−21 Å$^2$.

## Conclusions

On the basis of the experimental and simulation results, we conclude that the transition observed at $\Pi_p$ is the shift from polymer chains existing as a uniform monolayer to forming multilayer regions and eventually a multilayered system.

For very low surface pressures, each polymer molecule exists as an isolated collapsed disk. From our isotherm scalings in this regime, $\nu \approx 0.53$, suggesting that the air/water interface behaves approximately as a $\Theta$ solvent for PtBMA. As we compress the monolayer and bring the disks closer together, eventually they will begin to collide with other disks, generating the surface pressure rise observed when the available area is roughly 27 Å$^2$ monomer$^{-1}$. It is reasonable that the viscous component of the surface shear modulus would dominate this regime, as we observed, since the disks should be able to move fairly freely past one another when a stress is applied. Upon further compression, these disks collide more frequently, resulting in an increased surface pressure. In the plateau region, when $\Pi$ reaches $\Pi_p$, even though the area available for each chain is continuously decreasing, surface pressure remains constant. We interpret this as the region when a full monolayer has been essentially filled, and mono-

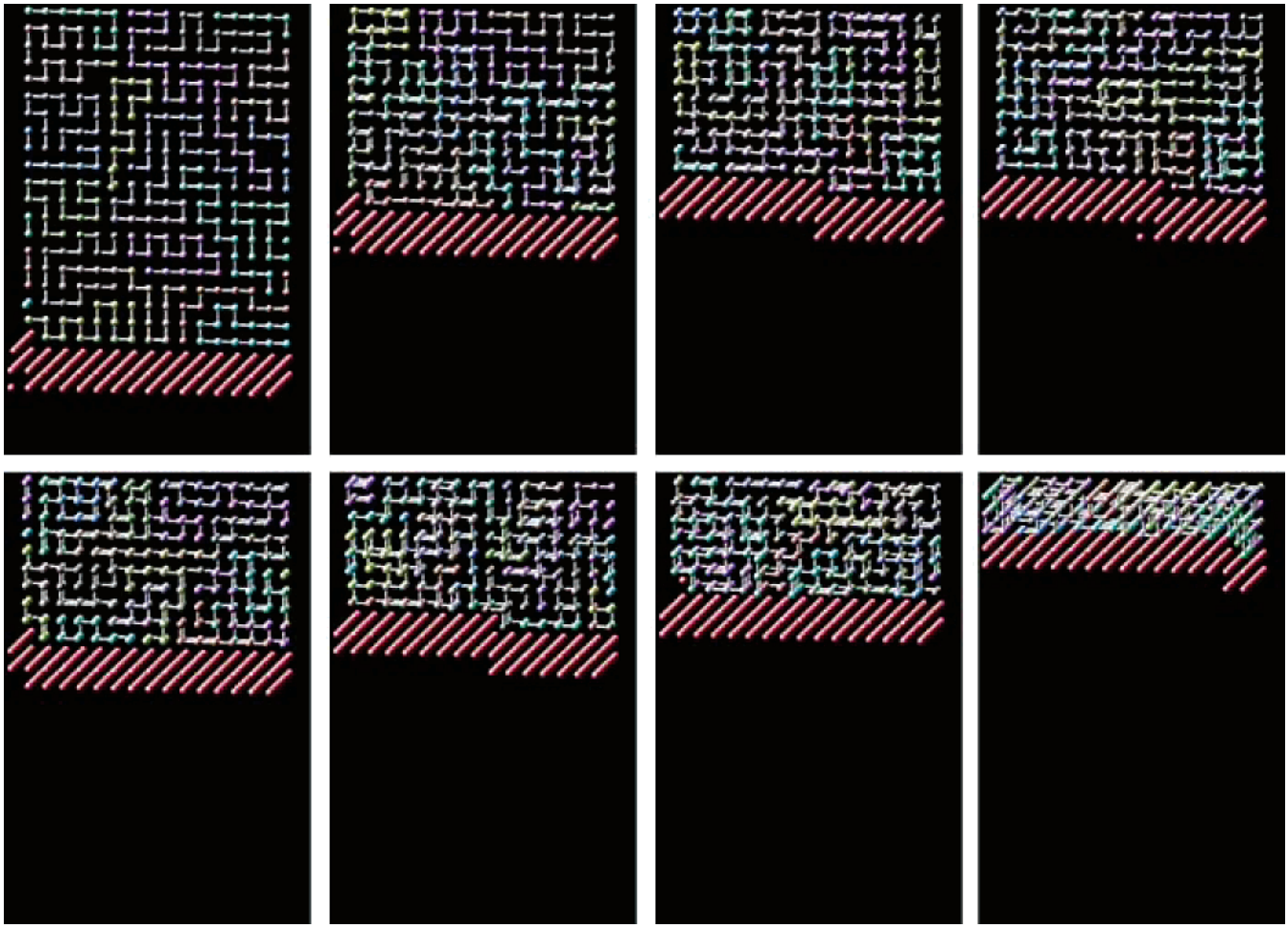

**Figure 13.** Snapshots of configurations for a representative computer-simulated system as a function of increasing pressure. The simulated moving barrier is shown compressing the polymer system. The density$^{-1}$ values corresponding to these (left−right, top−bottom) are 0.99, 0.68, 0.55, 0.51, 0.50, 0.44, 0.35, and 0.16.

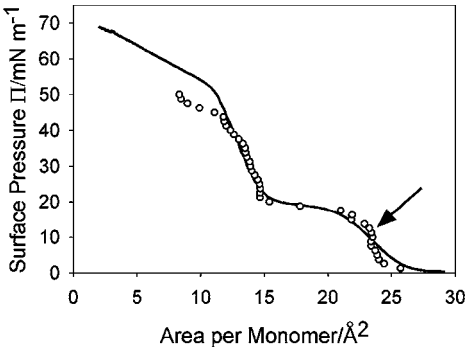


**Figure 14.** Experimental (—) and simulated (○) isotherms are shown on the same axes, showing a general agreement between the shapes. The simulated values have been scaled and shifted to provide a more quantitative estimate. The arrow marks a nominal density of unity in the simulation.

mer units are being squeezed up into a second layer. This behavior will relieve the stress applied by the compressing barriers. Above $\Pi_p$, the film continues to exist as a multilayered system, with increasing numbers of chain segments existing in higher order layers. Once a multilayer is present, entanglements can begin to form, dramatically increasing the elasticity of the film, as observed. The change in compressibility at high surface pressure could mark the complete filling of a second layer and the formation of additional layers. At this point, the available area during compression is changing at a rapid rate, and the observed behavior is likely quite far from equilibrium. Despite this, the upper branch of the isotherms extrapolates to intersect the surface pressure axis near 72.8 mN m$^{-1}$. This suggests that the polymer chains ultimately form a solid film with zero surface tension. If this is the case, we are able to observe a broad spectrum of systems—from a dilute 2D gas to bulk polymer film—in a single experiment. It is interesting to consider why a multilayer configuration leads to the observed molecular weight independence of the surface shear viscosity. We are not aware of any scaling arguments that support this observation and cannot yet rule out that these results are an experimental artifact.

The slight dip and reduced plateau pressure observed during expansion cycles of the hysteresis experiments can also be explained by this model. As the barriers are expanded, concentration gradients will drive the polymer chains away from one another to equilibrate the full available surface. However, in order for this to occur, the chains must disentangle. This process would likely require a significant amount of time, and this may be the justification for the observed dip in the expansion isotherms. Also, as the tightly compressed system relaxes to fill the surface, we suspect that some entangled domains persist for some time, packing together more efficiently than during compression. This could explain the textured appearance of the surface observed by BAM. Recall that this roughness was only observed

at very high surface pressures during compression but that it remained during expansion until the plateau was reached. By leaving more of the bare A/W interface exposed during expansion, the surface pressure will also be lower throughout the plateau region than during the compression plateau.

We have also considered an additional molecular justification for the plateau observed in the $\Pi-A$ isotherm. While the formation of a multilayered system seems to explain the experiments conducted thus far, we are still taking into account the possibility that the plateau results from a system where the monomer units lie flat on the interface at low pressure, then flip up as available space becomes more limited. This might occur if the sidearm group on each monomer—or some part of the arm—was bound less strongly to the interface. This mechanism would relieve the stress being applied to the system during compression, and the transition would also occur at the same areas as those observed. After all the monomer units have undergone this transition, the plateau will end, and the moving barriers will attempt to compress the newly oriented system. Preliminary simulations of this model show a plateau transition as expected, and we are investigating the feasibility of this mechanism.

We feel that the phenomena observed in this work are generally applicable to fluid/fluid systems stabilized by polymer surfactants with 2D conformations. Specifically, the proposed transition could suggest that different mechanisms are responsible for emulsion stabilization in various concentration regimes, where polymer conformation may be dissimilar. At low surface concentration, where polymer chains exist as independent disks, film drainage flow can easily move the molecules past one another, creating concentration gradients. The resulting Marangoni stresses could create a counterflow that prevents drop coalescence. At high surface concentrations, when the chains exist as an entangled, elastic network, drainage flow cannot easily move the molecules apart. Therefore, in this regime, it is more likely that the polymers provide stability by the formation of a solidlike shell on the interfaces.

By using surface rheological measurements together with computer simulation experiments, we have studied the behavior of polymer systems confined to 2D. In particular, we focus on the differences in the properties of PtBMA films above and below the plateau surface pressure, where a phase transition is suspected to take place. We have shown that there are significant differences in film properties around this changeover, and we suggest that this may mark the formation of a multilayer polymer film at the air/water interface. Hopefully these results can help elucidate the origins of viscoelasticity in two-dimensional polymer systems and aid in the understanding of polymer-stabilized emulsions and foams.

**Acknowledgment.** The authors gratefully acknowledge Grant NSF/DMR-0237247 and the Center on Polymer Interfaces and Macromolecular Assemblies (CPIMA) for funding this research and Rachel E. Kurtz for helpful conversations.

## References and Notes

(1) Yethiraj, A. *Macromolecules* **2003**, *36*, 5854−5862.
(2) Ostrovsky, B.; Smith, M. A.; Bar-Yam, Y. *Int. J. Mod. Phys. C* **1997**, *8*, 931−939.
(3) Adamson, A. W.; Gast, A. P. *Physical Chemistry of Surfaces*, 6th ed.; Wiley: New York, 1997.
(4) Poindexter, M.; Zaki, N.; Kilpatrick, P.; Marsh, S.; Emmons, D. *Energy Fuels* **2002**, *16*, 700−710.
(5) McLean, J.; Kilpatrick, P. *J. Colloid Interface Sci.* **1997**, *189*, 242−253.
(6) de Gennes, P. G. *Scaling Concepts in Polymer Physics*; Cornell University Press: Ithaca, NY, 1993.
(7) Carmesin, I.; Kremer, K. *J. Phys. (Paris)* **1990**, *51*, 915−932.
(8) Semenov, A. N.; Johner, A. *Eur. Phys. J. E* **2003**, *12*, 469−480.
(9) Peng, J. B.; Barnes, G. T. *Langmuir* **1991**, *7*, 1749−1754.
(10) Naito, K. *J. Colloid Interface Sci.* **1989**, *131*, 218−225.
(11) Maier, B.; Radler, J. O. *Phys. Rev. Lett.* **1999**, *82*, 1911−1914.
(12) Maier, B.; Radler, J. O. *Macromolecules* **2000**, *33*, 7185−7194.
(13) Maier, B.; Radler, J. O. *Macromolecules* **2001**, *34*, 5723−5724.
(14) Vilanove, R.; Rondelez, F. *Phys. Rev. Lett.* **1980**, *45*, 1502−1505.
(15) Poupinet, D.; Vilanove, R.; Rondelez, F. *Macromolecules* **1989**, *22*, 2491−2496.
(16) Vilanove, R.; Poupinet, D.; Rondelez, F. *Macromolecules* **1988**, *21*, 2880−2887.
(17) Sacchetti, M. In *Pharmacy*; University of Wisconsin−Madison: Madison, WI, 1992.
(18) Sacchetti, M.; Yu, H.; Zografi, G. *Langmuir* **1993**, *9*, 2168−2171.
(19) Sato, N.; Ito, S.; Yamamoto, M. *Macromolecules* **1998**, *31*, 2673−2675.
(20) Barentin, C.; Muller, P.; Ybert, C.; Joanny, J. F.; di Meglio, J. M. *Eur. Phys. J. E* **2000**, *2*, 153−159.
(21) Monroy, F.; Hilles, H. M.; Ortega, F.; Rubio, R. G. *Phys. Rev. Lett.* **2003**, *91*, 268302−268304.
(22) Esker, A. R.; Zhang, L.-H.; Sauer, B. B.; Lee, W.; Yu, H. *Colloids Surf. A* **2000**, *171*, 131−148.
(23) Cicuta, P.; Hopkinson, I. *Europhys. Lett.* **2004**, *68*, 65−71.
(24) Gaines, G. L. *Insoluble Monolayers at Liquid−Gas Interfaces*; Wiley: New York, 1966.
(25) Brooks, C. F.; Fuller, G. G.; Frank, C. W.; Robertson, C. R. *Langmuir* **1999**, *15*, 2450−2459.
(26) Wall, F. T.; Mandel, F. *J. Chem. Phys.* **1975**, *63*, 4592−4595.
(27) Verdier, P. H.; Stockmayer, W. H. *J. Chem. Phys.* **1962**, *36*, 227.
(28) Lovett, R.; Baus, M. *J. Chem. Phys.* **1991**, *95*, 1991−1994.
(29) Dickman, R. *J. Chem. Phys.* **1987**, *87*, 2246−2248.
(30) Landau, L. D.; Lifshitz, E. M. *Statistical Physics*, 2nd ed.; Pergamon: New York, 1978.

MA050061N